

Article

Influence of Low Inlet Pressure and Temperature on the Compressor Map Limits of Electrical Turbo Chargers for Airborne Fuel Cell Applications

Jonas Schröter , Daniel Frank, Valentin Radke, Christiane Bauer , Josef Kallo and Caroline Willich * 

Institute for Energy Conversion and Storage, Ulm University, Albert-Einstein-Allee 47, 89081 Ulm, Germany; jonas.schroeter@uni-ulm.de (J.S.); daniel.frank@uni-ulm.de (D.F.); valentin.radke@uni-ulm.de (V.R.); christiane.bauer@uni-ulm.de (C.B.); josef.kallo@uni-ulm.de (J.K.)

* Correspondence: caroline.willich@uni-ulm.de

Abstract: For the optimal high-efficiency operation of a PEM fuel cell system, the temperature, pressure, humidity and mass flow of the supplied air must be tuned to the fuel cell stack requirements. Especially for aircraft applications, this requires a thorough understanding of the fuel cell air supply system behavior and how it changes when the ambient pressure is below 1 bar(a) during flight. This work investigates the influence of low inlet pressures and varying inlet temperatures on the compression map of an electrical turbo charger. This is especially relevant in airborne fuel cell application and not much literature can be found on that topic. Compressor limits are evaluated experimentally and theoretically. The theory of mass flow and speed correction is compared to experimental findings and found to be applicable for the surge and speed limit of the investigated turbo chargers as long as the compressor map is not limited by the power of the electric motor and inverter. Based on this, a prediction of the compressor map for altitudes up to 10,000 m is made with the help of a developed software tool.

Keywords: compressor map; low pressure; pressurized fuel cell



Citation: Schröter, J.; Frank, D.; Radke, V.; Bauer, C.; Kallo, J.; Willich, C. Influence of Low Inlet Pressure and Temperature on the Compressor Map Limits of Electrical Turbo Chargers for Airborne Fuel Cell Applications. *Energies* **2022**, *15*, 2896. <https://doi.org/10.3390/en15082896>

Academic Editors: Bahman Shabani and Mahesh Suryawanshi

Received: 21 March 2022

Accepted: 11 April 2022

Published: 15 April 2022

Publisher's Note: MDPI stays neutral with regard to jurisdictional claims in published maps and institutional affiliations.



Copyright: © 2022 by the authors. Licensee MDPI, Basel, Switzerland. This article is an open access article distributed under the terms and conditions of the Creative Commons Attribution (CC BY) license (<https://creativecommons.org/licenses/by/4.0/>).

1. Introduction

Fuel cell-powered airplanes provide the potential to significantly reduce global greenhouse gas emissions in aviation [1,2]. The requirements related to system mass and volume-specific energy density, power and security are very demanding compared to conventional fields of fuel cell application [3–5].

One of the biggest differences compared to automotive applications is the greater variation in ambient conditions. While the pressure on the ground is around 1 bar(a), depending on the location and weather, ambient pressure during flight decreases significantly with higher flight altitudes. According to the International Standard Atmosphere [6], ambient pressure is decreased to 0.26 bar(a) at a height of 10 km, which is typical for long-range flights [7]. Temperature also decreases with altitude. For the mentioned altitude of 10 km, temperature decreases to $-50\text{ }^{\circ}\text{C}$.

The performance of fuel cells increases with higher operation pressures. Lee et al. [2] simulated a pressurized air-cooled fuel cell stack and found an improvement in stack power by pressurizing the inlet air up to 5 atm. The lower air velocity resulting from higher air pressure mitigated the electrolyte dehydration. Pressurization also led to a more uniform current density distribution through reduced reactant depletion. Furthermore, the activation overpotential and the ohmic losses were reduced with increased pressure. These results are confirmed by other studies [4,5,8–10].

The changes in inlet conditions during flight affect the air supply to the fuel cell system. In order to ensure stable and powerful operation, an air supply system is needed that enables control of the inlet pressure of the stack. In an all-electric system an electrical

turbo charger is typically used to adjust the pressure level [8,11–13], but it is necessary to take into account the varying performance of a given turbo charger depending on the inlet conditions [9,14].

Kurzke et al. [15–17] used the corrected mass flow and speed to predict compressor maps of conventional gas turbines for flight-relevant conditions from known lines in the compressor map, obtained at standard conditions. They stated that the analytical prediction of the pressure ratio is difficult and therefore used empirical data for their model. The predictions matched well with their measured compressor maps. Leufven et al. [18] also used the corrected mass flow and speed correction derived from dimensionless numbers to predict the compressor map for a gas turbine. Their model fit well with the measured data from their gas turbine test bench.

Not much attention has been paid thus far to the effects of ambient pressure and temperature changes on the limits due to power and the maximum speed of electric driven turbo chargers, as the relevance of this topic only recently arose with the growing interest in pressurized PEM fuel cells in recent years. The limiting factors for the compressor maps of gas turbines and electrical compressors are not necessarily the same, because the power sources for driving the compression are different. Gas turbines use the expansion of the exhaust gas in a turbine, while electric compressors use an electric motor. Therefore, there is a need to investigate the effects that limit the operation of electrical turbo compressors for low inlet pressures and temperatures, as this is relevant for airborne fuel cell applications.

This work investigates the shift of the compressor map and its limitations for electrically driven turbo chargers, aiming at an application in a fuel cell air supply in aviation. The focus lays on applying and confirming mass flow and speed correction in order to predict altitude dependent compressor map shifts. For this reason, the Rotrex EK10AA and the Fischer 150k fuel cell air compressor are used as representatives of commercially available electrical turbo chargers and are evaluated experimentally under simulated flight conditions in a climate chamber. The influences of pressure and temperature changes are tested separately as well as in combination, as occurs during real flight conditions. The experimental data is compared to analytical data obtained via a developed software tool which calculates corrected mass flow and corrected speed from compressor maps at ground conditions. This comparison shows in which cases the mass and speed correction terms, known from gas turbines, correctly describe the compressor map shift of electrical turbo chargers, and can be used for predictions of the compressor map changes for high altitudes. The results also show that for electrical compressors, whose performance is limited by the inverter power, the performance at high altitude is underestimated when using the mass and speed correction terms.

2. Operational Map of Electrical Turbo Compressors

2.1. Compressor Map Limits

The typical compressor map of an electrical turbo compressor shows the pressure ratio between in and outlet pressure over the air mass flow. This map is in principle limited by four relevant effects [19–25]: the surge limit, the choke limit, the speed limit and the power limit.

The surge line limits the compressor map at low mass flows and high pressure ratios. This limit is relevant for every turbo compressor. At the surge limit, a stall of the flow occurs which leads to an air oscillation and reversed flow that can cause severe damage to the compressor, especially in cases of air bearing.

The choke limit depends on the geometry of the compressor and is only relevant for some compressors. Once the air flowing through the blades and volute reaches the speed of sound, it cannot be further accelerated. Therefore, the maximum possible mass flow is reached in this point and the choke line limits the compressor map at higher mass flows.

The speed limit protects the compressor from structural damages by limiting the maximum impeller speed through the implementation of the inverter control. The speed limit therefore limits the compressor map at higher pressure ratios and at higher mass flows.

The power limit is only relevant for some electrical turbo chargers and depends on the manufacturer's technical configuration of the motor. If the power limit is reached, the inverter or the electrical motor prevents a further acceleration of the impeller. For some turbo charger/inverter combinations a minimum voltage is needed to reach a certain speed. Often a maximum current limit is implemented into the system for thermal reasons. As the inlet pressure decreases, the air mass flow also decreases, and therefore less power is required for compression [9]. This means that the power limit becomes less important at lower inlet pressures. In this case, the speed limit might become the relevant limit of the compressor map.

2.2. Compressor Map Prediction according to Corrected Mass Flow

The considered application for electrical turbo chargers in this work is the supply of air to a fuel cell in aviation. For this reason, the absolute compressor outlet pressure, which correlates to the fuel cell inlet pressure, is the variable of interest. The term absolute compressor map is used in this work to describe a map of the absolute outlet pressure of the turbo charger over the mass flow.

The prediction of the absolute compressor map for gas turbines in literature [15,17,18,20,21] is usually done with the help of a universal compressor map showing the pressure ratio over the air mass flow for defined standard conditions and the formula for mass flow correction Equation (5), assuming Mach similarity.

The Mach number in flow direction M_f is the ratio of flow velocity v to the speed of sound c .

$$M_f = \frac{v}{c} = \frac{v}{\sqrt{\kappa R_s T}} \rightarrow v = M_f \sqrt{\kappa R_s T} \quad (1)$$

where c is expressed through the adiabatic index for air $\kappa = 1.4$, the specific gas constant for air $R_s = 287 \frac{J}{kg \cdot K}$; and the air temperature.

The density of air ρ can be calculated from the ideal gas law with the pressure p ; the gas constant R_s ; and the air temperature T .

$$\rho = \frac{p}{R_s T} \quad (2)$$

Using the cross sectional area A , Equations (1) and (2) the air mass flow through the compressor can be expressed according to Equation (3).

$$\dot{m} = \rho A v = \frac{p}{R_s T} A \left(M_f \sqrt{\kappa R_s T} \right) \quad (3)$$

Comparing the air mass flow for two different inlet temperatures and pressures indexed "0" and "1" leads to

$$\frac{\dot{m}_1}{\dot{m}_0} = \frac{\frac{p_1}{R_s T_1} A \left(M_f \sqrt{\kappa R_s T_1} \right)}{\frac{p_0}{R_s T_0} A \left(M_f \sqrt{\kappa R_s T_0} \right)} = \frac{p_1 \sqrt{T_0}}{p_0 \sqrt{T_1}} \quad (4)$$

$$m_1 = m_0 \frac{p_1 \sqrt{T_0}}{p_0 \sqrt{T_1}} \quad (5)$$

Equation (5) is named mass flow correction and can be used to predict the compressor behavior for varying inlet conditions. The mass flow correction is combined with a speed correction for varying inlet temperatures, also derived from Mach similarity. For the speed correction, the radial Mach number is the relevant parameter [20]. In this case, the flow velocity v in Equation (1) can be expressed by the radius r times the rotation speed to get an expression for the radial Mach number M_r .

$$M_r = \frac{v}{c} = \frac{r \omega}{\sqrt{\kappa R_s T}} \quad (6)$$

Comparing two different inlet temperatures and rearranging Equation (6) to be similar to Equation (4) leads to the speed correction Equation (7),

$$\omega_1 = \frac{\omega_0 \cdot \sqrt{T_1}}{\sqrt{T_0}} \quad (7)$$

where ω_1 is the assigned speed for T_1 , taking the speed ω_0 at temperature T_0 as the reference point. Varying inlet pressures do not affect the corrected speed.

3. Experimental Setup

To validate the developed equation, experimental tests were performed with an EK10AA turbo charger (Rotrex A/S, Ishøj, Denmark) [23] and an EMTC-150K AIR (FISCHER Fuel Cell Compressor AG, Herzogenbuchsee, Switzerland) [21] in a custom-made climate chamber [26]. The test bench setup, shown in Figure 1, was similar to the one described in [9]. Filtered ambient air was compressed with the specified electrical turbo charger. The heated air was cooled with an air-to-liquid intercooler before it passed the mass flow control valve. Sensors measured the compressors' static in- and outlet pressures (PT0517 and PT5504, ifm electronic GmbH, Essen, Germany) and temperatures (HFM5, Robert Bosch GmbH, Germany and TM4101 ifm electronic GmbH, Essen, Germany) as well as the air mass flow (HFM5, Robert Bosch GmbH, Gerlingen, Germany). Compressor speed and the state of the throttle valve were set manually in the control software. Each curve was recorded at its respective compressor speed. The maximum possible speed was 140 krpm for the Rotrex and 150 krpm for the Fischer compressor.

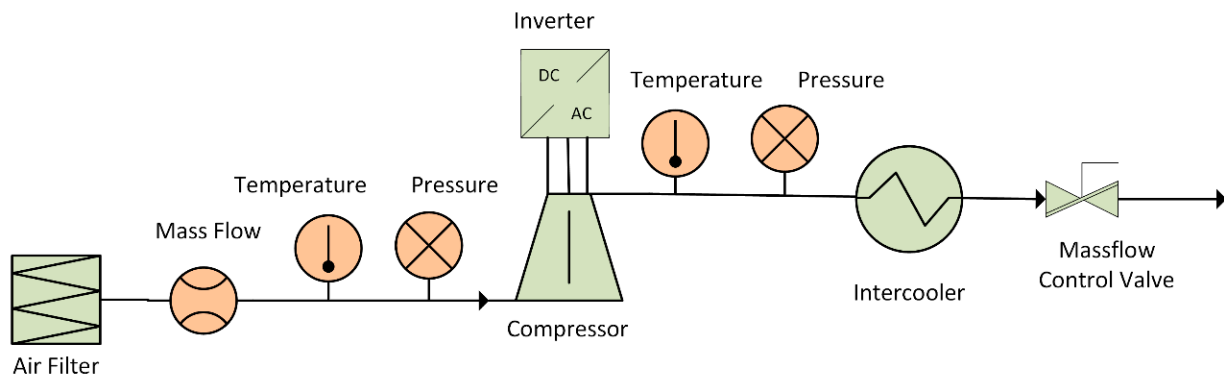


Figure 1. Schematic of the test bench setup, including air filter, compressor with inverter, intercooler, mass flow control valve and sensors.

According to Bernoulli's principle Equation (8), the dynamic pressure p_{dyn} calculated from mass flow and density was added to the measured static pressure p_{sta} to obtain the total pressure p_{tot} .

$$p_{tot} = p_{sta} + p_{dyn} = p_{stat} + \frac{1}{2} \cdot \frac{R_S \cdot T \cdot \dot{m}^2}{p_{sta} \cdot \pi^2 \cdot r^4} \quad (8)$$

Compressor outlet pressures were measured for inlet pressures of 940, 700 and 500 mbar(a) \pm 20 mbar and inlet temperatures of $-10, 5, 20$ and $40 \text{ }^\circ\text{C} \pm 4 \text{ }^\circ\text{C}$. In a further experiment, variation of inlet pressure and temperature were combined according to Table 1 to simulate the operating conditions of real flight altitudes.

Table 1. Values used for simulated altitude, oriented towards the international standard atmosphere.

Altitude/m.	Pressure/mbar(a)	Temperature/°C
600	935	11
1000	900	8
2000	800	2
3000	700	−5
4000	580	−11

4. Results and Discussion

4.1. Pressure and Temperature Dependence of the Compressor Map

For the following considerations, the measurements with the Rotrex EK10AA turbo compressor were evaluated because its compressor map is not determined by the power limit. Figure 2 shows the measured outlet pressures over the air mass flow for varying compressor inlet pressures (940 mbar, 700 mbar and 500 mbar) and rotational speeds of 120 and 140 krpm. These speeds were chosen because they represent the upper, application-relevant part of the compressor map. The observed shifts in pressure and mass flow for constant speed were valid for lower speeds in the same way. Points close to the surge line were avoided and only tested for the combined pressure and temperature variations since it was not clear how much mechanical overstressing the compressor could handle.

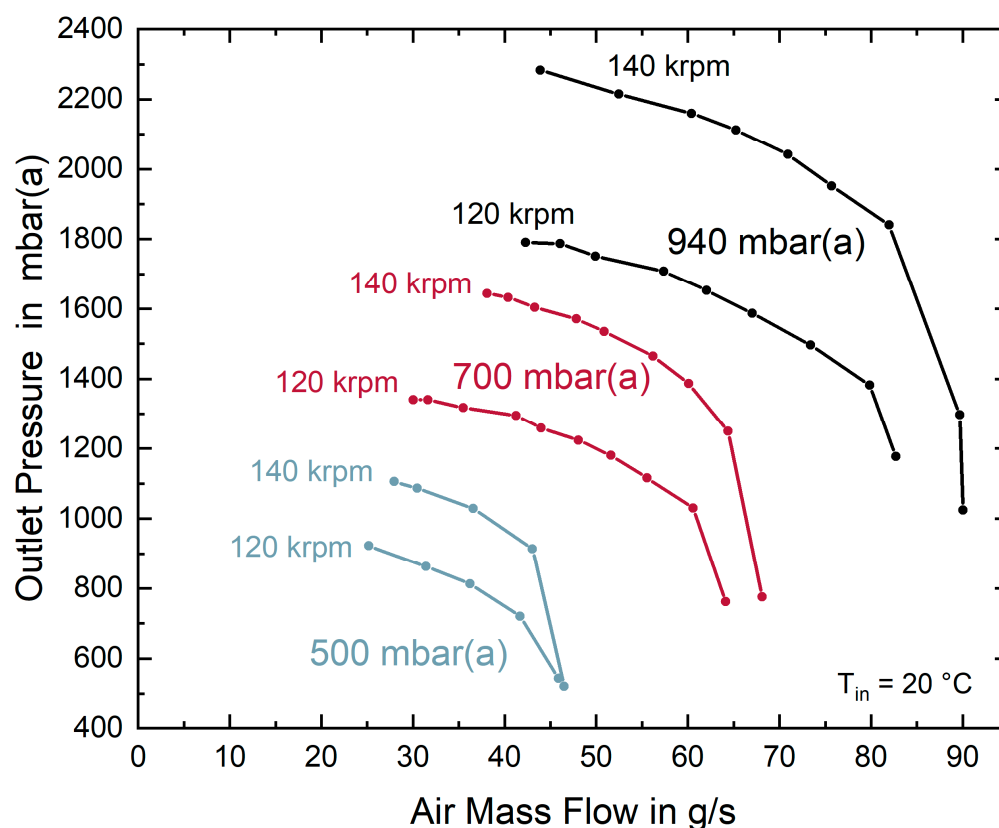


Figure 2. Absolute compressor map for 940, 700 and 500 mbar(a); inlet pressure and compressor speeds of 140 and 120 krpm; and 20 °C inlet temperature.

Figure 2 shows clearly that decreasing the inlet pressure led to a decrease in measured outlet pressure for the same air mass flow over the full compressor map, as was expected. For 140 krpm and an inlet pressure decrease from 940 mbar(a) to 700 mbar(a), the outlet pressure was reduced by more than 500 mbar for all mass flows. Further lowering to 500 mbar(a) inlet pressure led to an additional decrease of about 600 mbar for the same mass flow. The maximum air mass flow provided by the compressor also changed with inlet

pressure. The maximum air mass flow reduced from 90 g/s for 940 mbar(a) inlet pressure to 69 g/s for 700 mbar(a) and 47 g/s for 500 mbar(a). A similar behavior of outlet pressure and mass flow reduction was observed for all compressor speeds. The absolute outlet pressure difference for varying inlet pressures was smaller for lower compressor speeds. For example, for 120 krpm and 50 g/s, the difference between 940 mbar(a) and 700 mbar(a) was 560 mbar, compared to 700 mbar for 940 mbar(a) inlet pressure. The reason for this was a lower compression ratio at lower speeds and a resulting lower absolute difference.

Figure 3 shows the outlet pressure curves for rotational speeds of 120 and 140 krpm for four different air inlet temperatures ($-10\text{ }^{\circ}\text{C}$, $5\text{ }^{\circ}\text{C}$, $20\text{ }^{\circ}\text{C}$ and $40\text{ }^{\circ}\text{C}$).

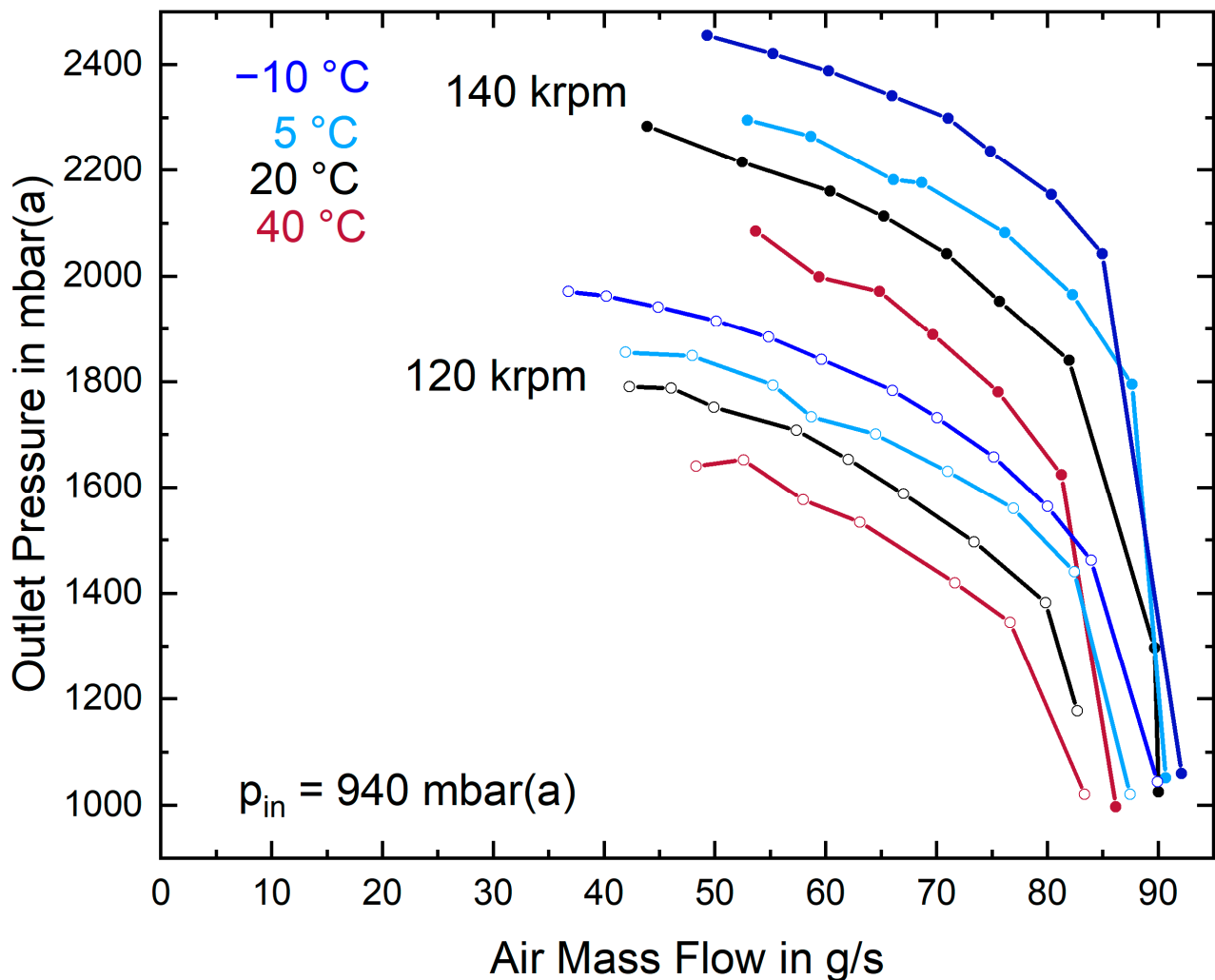


Figure 3. Absolute compressor map for varying inlet temperatures of $-10\text{ }^{\circ}\text{C}$ (dark blue), $5\text{ }^{\circ}\text{C}$ (light blue), $20\text{ }^{\circ}\text{C}$ (black) and $40\text{ }^{\circ}\text{C}$ (red) and varying compressor speeds of 120 krpm (empty points) and 140 krpm (filled points).

From the measured curves, it can be seen that lower inlet temperatures enabled higher compressor outlet pressures. For the maximum compressor speed, a 50 K temperature decrease from $40\text{ }^{\circ}\text{C}$ to $-10\text{ }^{\circ}\text{C}$ led to a higher outlet pressure of about 400 mbar for all mass flows. Furthermore, the maximum possible mass flow increased from 86 g/s to 92 g/s. These influences of the inlet temperature were also confirmed by the measurements for $5\text{ }^{\circ}\text{C}$ and $20\text{ }^{\circ}\text{C}$. For lower compressor speeds, the difference in absolute outlet pressure again decreased because of the lower pressure ratios, as described for varying inlet pressures.

Figures 2 and 3 show that the inlet pressure and temperature both have a significant influence on the compressor outlet pressure and need to be considered for a fuel cell system in airplane applications.

4.2. Corrected Mass Flow

In order to compare the measured results to the theory of corrected mass flow calculation, the measurements were corrected with Equations (5) and (7) to 940 mbar(a) and 20 °C, as shown in Figure 4. For the speed correction required for varying inlet temperatures, it was necessary to use curves with different speeds than the measured ones. A linear interpolation between 100 and 140 krpm was used to correct the speeds for the 120 krpm curves and a linear interpolation between 120 and 140 krpm was used to correct the 140 krpm curves. In reality, an exponential behavior would be expected, but the error made by using the much simpler linear interpolation was estimated to be below 5%, and thus negligible compared to the measurement error. An interpolation is always necessary if the compressor limits are corrected at lower inlet temperatures. For the 40 °C curve, the corrected speed is 145 krpm which would not be possible with the measured compressor.

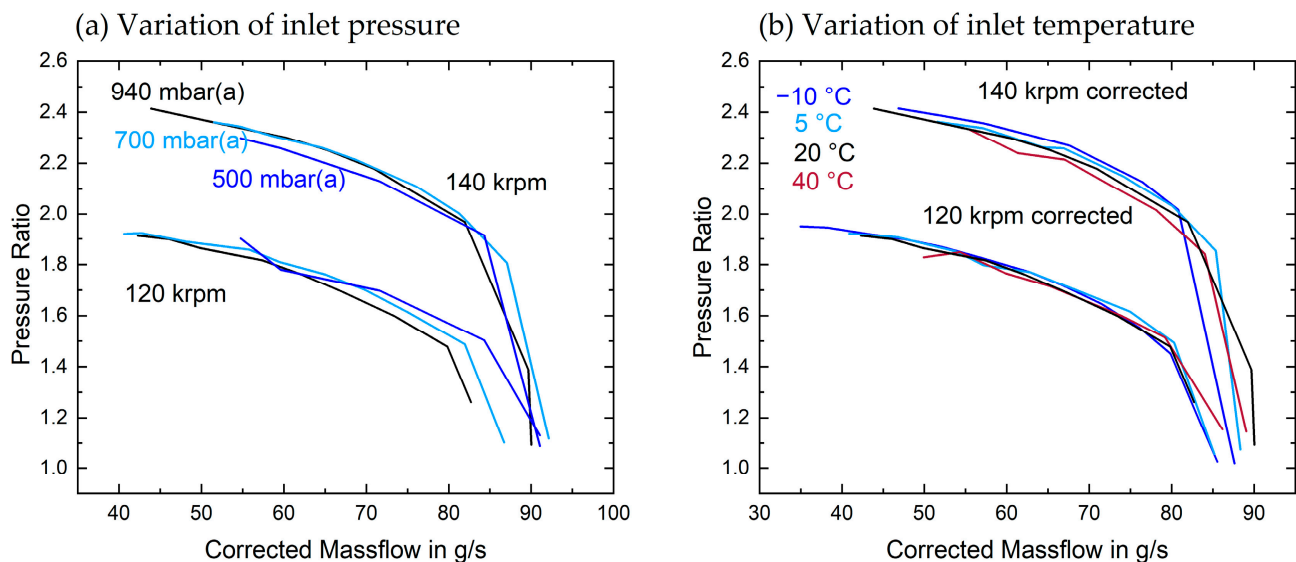


Figure 4. (a) Pressure ratio over corrected mass flow for measurements with 940 mbar(a) (black), 700 mbar(a) (light blue) and 500 mbar(a) (dark blue) inlet pressure at 20 °C, corrected to 20 °C and 940 mbar(a). (b) Pressure ratio over corrected mass flow for measurements with −10 °C (dark blue), 20 °C (black), 5 °C (light blue) and 40 °C (red) inlet temperature at 940 mbar(a), corrected to 20 °C and 940 mbar(a).

The resulting curves matched well within the range of the measurement error. Therefore, it can be concluded that Equations (5) and (7) correctly described the shift of the compressor map for the speed limit, as this is the relevant limit for the observed measurements.

4.3. Flight Conditions

During a real flight, pressure and temperature changes occur simultaneously. In order to assess the behavior for this combined change, tests were performed in the climate chamber emulating realistic flight conditions, as given in Table 1.

Figure 5 shows the compressor map using corrected mass flow and pressure ratio for different altitudes according to the standard atmosphere [6], as given in Table 1.

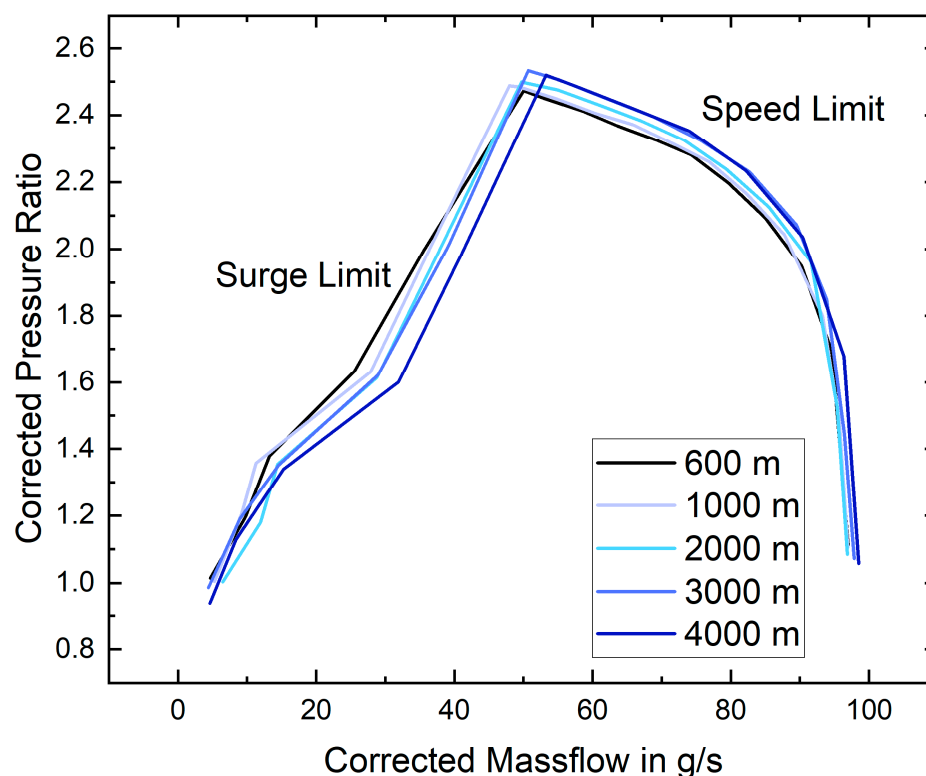


Figure 5. Pressure ratio over corrected air mass flow for measurements with simulated altitudes of 600, 1000, 2000, 3000 and 4000 m corrected to 0 m (15 °C, 1000 mbar(a)).

The correction terms, Equations (5) and (7), describe the behavior of the speed limit with varying altitudes well in the range of error, and it can be concluded that the correction terms are also valid for combined temperature and pressure changes with increasing altitude. Therefore, these equations can be used to calculate all relevant limits for the examined compressor. Of course, this is only valid if the speed, and not the power, limits the compressor map such as for the investigated Rotrex EK10AA.

4.4. Influence of Power Limit on the Compressor Map at Varying Inlet Pressures

For the second examined compressor, the Fischer 150k, the power limit, which is implemented in the inverter controller, limits part of the operation map of the compressor. In this case, the correction terms Equations (5) and (7) cannot be used to describe the operation range. Figure 6 shows the experimentally obtained values of the pressure ratio over the corrected air mass flow for different inlet pressures.

It can be observed that the compressor map at high inlet pressures was limited at higher air mass flows and pressures by the maximum power that the motor can provide. Once this power limit was reached, further acceleration of the impeller was prevented by the inverter. As mentioned previously, the power limit becomes less important with lower inlet pressures since the power depends on the air mass flow [9], which decreases with low inlet pressures. It can be seen from Figure 6 that at inlet pressures lower than 700 mbar(a), the compressor map of the investigated Fischer 150k was no longer determined by the motor power and the speed limit became the only relevant limit.

For the examined Fischer 150k, the power limit also depends on the pressure ratio since it varied between 4.5 and 5.3 kW during the measurements. Higher power was achieved at higher pressure ratios.

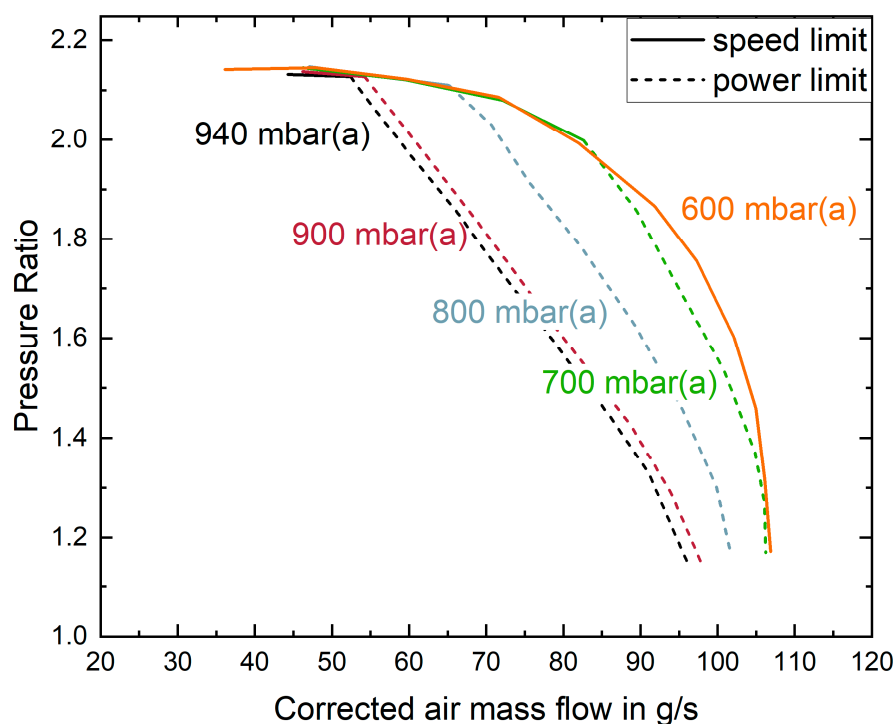


Figure 6. Corrected pressure ratios over corrected air mass flow for the measurements with the Fischer 150k compressor, for inlet pressures of 940, 900, 800, 700 and 600 mbar(a), corrected for 20 °C and 940 mbar(a). Dashed lines indicate the power limit.

4.5. Prediction of the Compressor Map

Using the mass and speed correction terms, the behavior of a compressor map without a power limit at even higher altitudes can be predicted. Based on Equations (5) and (7), a software tool (see Supplementary Material) was implemented in OriginLab to predict the changes of the absolute compressor map with altitude. The corresponding inlet pressure and temperature values are calculated according to the International Standard Atmosphere. The known surge and speed limits, often given in compressor data sheets, can be entered as data points and the mass and speed correction are used to calculate the new pressure and mass flow points for the desired altitude. For the speed correction, a linear fit through the origin is assumed. The error made by this assumption is less than 5% for the investigated compressors which is negligible compared to measurement errors. The resulting compressor map for the desired altitude is plotted automatically. The software tool is published together with this study.

Figure 7 shows the measured, as well as predicted values for the maximum reachable outlet pressure, the corresponding mass flow and the maximum possible air mass flow over altitude for the Rotrex EK10AA compressor, which is not limited by power.

It can be seen that the operation range regarding outlet pressure and air mass flow significantly decreases when going to higher altitudes. At an altitude of 5000 m, the point of maximum outlet pressure decreased from 2500 mbar(a) at 50 g/s to 1450 mbar(a) at 29 g/s compared to ground level. Going up to 10,000 m, which corresponds to −50 °C and 264 mbar(a), the maximum outlet pressure decreased further to 780 mbar(a) at 15 g/s. Furthermore, the maximum possible air mass flow decreased from 98 g/s at 0 m, to 55 g/s at 5000 m and to 29 g/s at 10,000 m. The measured points are in good agreement with the predicted points for the Rotrex EK10AA compressor.

The tool only works fine if the input operation map is not limited by the power, because in that case the speed limit is not determining the boundaries of the operational map. However, the maximum power can also be entered into the tool to calculate the power limit. To simplify the calculation, a constant efficiency of 60% [9] was assumed, which can

also be changed if necessary. The calculation of the power limit is only relevant for two cases: 1. If the speed limit is known and used as input and a power limit is implemented afterwards. 2. If the input reference compressor map is taken at low pressures without the presence of the power limit, but the performance at higher inlet pressures for which the power limit is relevant, is of interest.

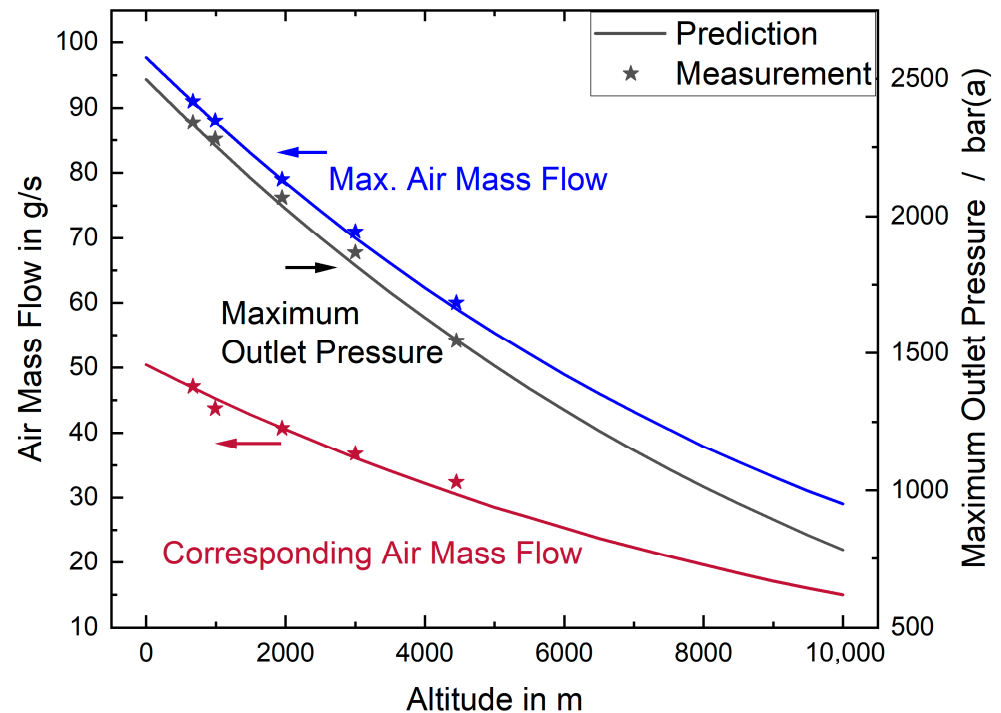


Figure 7. Predicted maximum pressure ratio with corresponding air mass flow and maximum air mass flow for the Rotrex EK10AA; measurement data are plotted in stars for comparison.

Figure 8 shows the measured compressor limit at 600 m as well as the measured and calculated limits for 4000 m. This change in altitude corresponds simultaneously to a change in pressure and temperature. Since the 600 m curve was measured closer to the surge limit than the 4000 m curve, the calculated curve for 4000 m contains points with a lower mass flow than the measured curve.

It can be seen that the prediction works fine in the range of error for the part of the compressor map that is limited by the speed limit. In contrast, the power limitation of the reference curve at 600 m leads to an underestimation of the compressor map for 4000 m because the power limit is used as input, although it becomes less relevant with increased altitude. As can be seen, the measured curve is only limited by the speed limit, and the correction only works for the parts of the compressor map that are not limited by the power.

If the surge and speed limit alone define the borders of the reference compressor map, the prediction according to the mass and speed correction, work reliably. This is shown by the good agreement of measured and calculated data presented in Figure 7, as well as for the very low mass flows in Figure 8. When using the mass and speed correction terms, only the available points of the reference compressor map are corrected. If points close to the surge line are missing, the tool cannot predict these points for other inlet conditions.

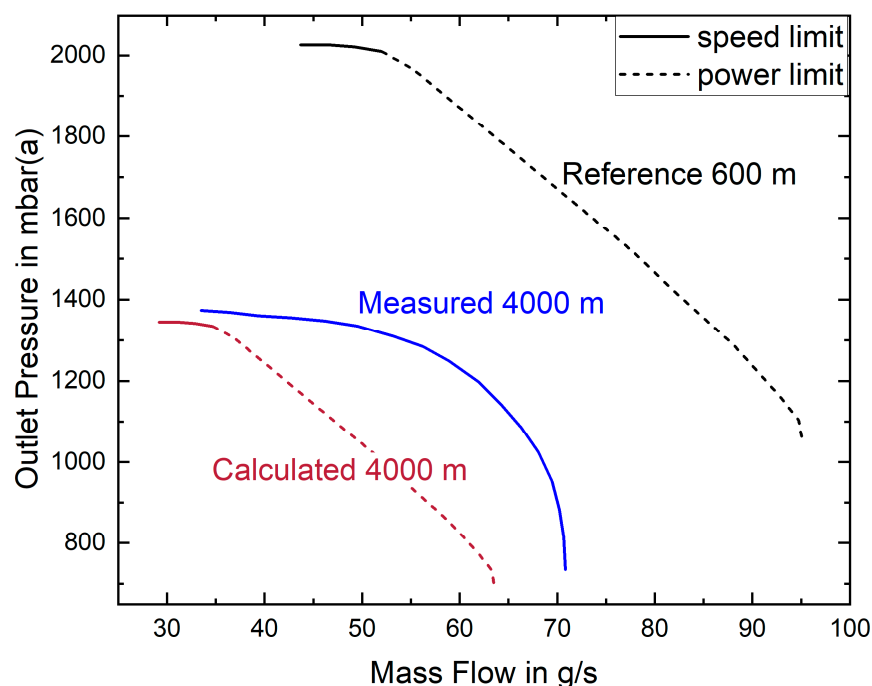


Figure 8. Measured compressor limit at 600 m and calculated corresponding limit at 4000 m, in comparison to the measured compressor limit for a 4000 m altitude for the Fischer 150k compressor. Speed limit is plotted in the solid line and the power limit is plotted in dashed lines.

5. Conclusions

This work examined the influence of varying inlet pressure and temperature resulting from varying flight altitudes on the compressor map of two electrical turbochargers. Two commercially available turbo compressors, the Rotrex EK10AA and the Fischer 150k, are tested in a custom-made climate chamber at different ambient temperatures, pressures and combinations of both, that simulate flight altitudes. Decreasing the inlet pressure leads to a decrease in the measured outlet pressure for the same air mass flow over the full compressor map, while lower inlet temperatures enable higher compressor outlet pressures, as is to be expected. The results of the Rotrex EK10AA were compared to the theory of corrected mass flow and speed and confirmed the applicability of corrected mass flow and corrected speed relationships for the speed and the surge limit of the compressor at varying flight altitudes. This allows the selection of electrical turbochargers for airborne fuel cell application with only one given compressor map, which is defined by the speed, choke and surge limit. Typically, manufacturers give the map for ground conditions. From this map the behavior of the compressor for other altitudes can be predicted.

Based on this, a software tool was developed to calculate the impact of altitude on the compressor map considering the combined change in pressure and temperature, and a prediction of the compressor map for up to 10,000 m altitude was given. The maximum possible outlet pressure and air mass flow range significantly decreased for elevated flight altitudes. The maximum outlet pressure and the maximum possible air mass flow for the investigated Rotrex EK10AA compressor dropped by 70% when going from sea level to 10,000 m.

However, for some commercially available compressors, like the examined Fischer 150k, the maximum power available from the motor and inverter limits the compressor map and corrected mass flow and speed can no longer be used for the prediction of the compressor map at low inlet pressures. This power limit becomes less relevant with increasing altitude, so using the mass and speed correction theory might underestimate the performance at high altitudes. In order to reliably predict the behavior at high altitudes the compressor map that is not limited by inverter or motor power has to be known.

The results gained in this study can be used to predict the operation range of a pressurized airborne fuel cell system. Further research is necessary to examine the effect of high altitude on the efficiency and power of the compressor and the corresponding fuel cell system.

Supplementary Materials: The following supporting information can be downloaded at: <https://www.mdpi.com/article/10.3390/en15082896/s1>, Video S1: Map prediction tool.

Author Contributions: Conceptualization, C.B. and C.W.; Data curation, Valentin Radke; Funding acquisition, C.B., J.K. and C.W.; Investigation, J.S., D.F. and V.R.; Methodology, J.S. and D.F.; Project administration, C.B.; Supervision, C.W.; Validation, J.S., D.F. and V.R.; Visualization, J.S.; Writing—original draft, J.S., D.F., V.R. and C.W.; Writing—review & editing, C.W. All authors have read and agreed to the published version of the manuscript.

Funding: This research was funded by the German Federal Ministry for Economic Affairs and Energy as part of the project HighV (20Y1701B) and the Federal Ministry for Transport and Digital Infrastructure as part of the project Go4Hy2 (03B10703A).

Institutional Review Board Statement: Not applicable.

Informed Consent Statement: Not applicable.

Data Availability Statement: Not applicable.

Acknowledgments: The authors want to thank Marcel Haag and Fatih Türk for their help in setting up the test bench and Florian Becker from DLR Hamburg for fruitful discussions.

Conflicts of Interest: The authors declare no conflict of interest.

Nomenclature

A	cross sectional area
c	speed of sound
\dot{m}	air mass flow
M_f	Mach number in flow direction
M_r	Mach number in radial direction
p	pressure
r	radius
R_s	specific gas constant for air
T	temperature
v	flow velocity
κ	adiabatic index for air
ρ	density of air
ω	rotation speed

References

1. EASA. European Aviation Environmental Report 2019. Available online: www.easa.europa.eu/eaer (accessed on 11 April 2022).
2. Lee, D.S.; Fahey, D.W.; Skowron, A.; Allen, M.R.; Burkhardt, U.; Chen, Q.; Doherty, S.J.; Freeman, S.; Forster, P.M.; Fuglestvedt, J.; et al. The contribution of global aviation to anthropogenic climate forcing for 2000 to 2018. *Atmos. Environ. (1994)* **2021**, *244*, 117834. [[CrossRef](#)] [[PubMed](#)]
3. Peters, R. *Brennstoffzellensysteme in der Luftfahrt*; Springer: Berlin/Heidelberg, Germany, 2015; ISBN 978-3-662-46797-8.
4. Flade, S.; Stephan, T.; Thalau, O.; Burberg, T.; Schirmer, J.; Kallo, J. Air Breathing PEM Fuel Cells in Aviation. *ECS Trans.* **2016**, *75*, 471–477. [[CrossRef](#)]
5. Werner, C.; Busemeyer, L.; Kallo, J. The impact of operating parameters and system architecture on the water management of a multifunctional PEMFC system. *Int. J. Hydrog. Energy* **2015**, *40*, 11595–11603. [[CrossRef](#)]
6. Heinkel, M. ICAO-Standardatmosphäre (ISA). Available online: www.dwd.de (accessed on 11 April 2022).
7. Joos/as. Lufthansa: Die Flotte des Kranichs. Available online: <https://www.flugrevue.de/zivil/groesste-deutsche-fluggesellschaft-lufthansa-die-flotte/> (accessed on 11 April 2022).
8. Schröder, M.; Becker, F.; Kallo, J.; Gentner, C. Optimal operating conditions of PEM fuel cells in commercial aircraft. *Int. J. Hydrog. Energy* **2021**, *46*, 33218–33240. [[CrossRef](#)]

9. Schröter, J.; Graf, T.; Frank, D.; Bauer, C.; Kallo, J.; Willich, C. Influence of pressure losses on compressor performance in a pressurized fuel cell air supply system for airplane applications. *Int. J. Hydrog. Energy* **2021**, *46*, 21151–21159. [CrossRef]
10. Wahdame, B.; Candusso, D.; Kauffmann, J.-M. Study of gas pressure and flow rate influences on a 500W PEM fuel cell, thanks to the experimental design methodology. *J. Power Sources* **2006**, *156*, 92–99. [CrossRef]
11. Pischinger, S.; Schönfelder, C.; Bornscheuer, W.; Kindl, H.; Wiartalla, A. Integrated Air Supply and Humidification Concepts for Fuel Cell Systems. In *SAE Technical Paper Series, Proceedings of the SAE 2001 World Congress, Detroit, Michigan, 5–8 March 2001*; SAE International: Warrendale, PA, USA, 2001.
12. Campanari, S.; Manzolini, G.; Beretti, A.; Wollrab, U. Performance Assessment of Turbocharged Pem Fuel Cell Systems for Civil Aircraft Onboard Power Production. *J. Eng. Gas Turbines Power* **2008**, *130*, 021701. [CrossRef]
13. Garrett Motion Inc. Hydrogen Fuel Cell Vehicles to Accelerate Electrification in the Global Auto Industry. Available online: www.garrettmotion.com (accessed on 11 April 2022).
14. Fröhlich, P. Development of an oil free turbo compressor for mobile fuel cell applications—challenges and results. In Proceedings of the Konferenzband der ersten FC³ Fuel Cell Conference, Chemnitz, Germany, 23–24 November 2019.
15. Kurzke, J.; Riegler, C. A New Compressor Map Scaling Procedure for Preliminary Conceptual Design of Gas Turbines. In *Volume 1: Aircraft Engine; Marine; Turbomachinery; Microturbines and Small Turbomachinery, Proceedings of the ASME Turbo Expo 2000: Power for Land, Sea, and Air, Munich, Germany, 8–11 May 2000*; American Society of Mechanical Engineers: New York, NY, USA, 2014; p. 05082000. ISBN 978-0-7918-7854-5.
16. Kurzke, J. Correlations Hidden in Compressor Maps. In Proceedings of the ASME 2011 Turbo Expo: Turbine Technical Conference and Exposition, Vancouver, BC, Canada, 6–10 June 2011.
17. Kurzke, J. Model Based Gas Turbine Parameter Corrections. In *Volume 1: Turbo Expo 2003, Proceedings of the ASME Turbo Expo 2003, Collocated with the 2003 International Joint Power Generation Conference, Atlanta, GA, USA, 16–19 June 2003*; American Society of Mechanical Engineers: New York, NY, USA, 2009; Volume 06162003, pp. 91–99. ISBN 0-7918-3684-3.
18. Leufven, O.; Eriksson, L. Engine Test Bench Turbo Mapping. In Proceedings of the SAE 2010 World Congress, Detroit, MI, USA, 13–15 April 2010; SAE International: Warrendale, PA, USA, 2010.
19. Garrett Motion Inc. Turbo Tech 103|Expert: Compressor Mapping. Available online: www.garrettmotion.com (accessed on 11 April 2022).
20. Volker, Gümmer. Lecture Flight Propulsion 1 and Gas Turbines: Establishing Mach No. Similitude. Munich, Germany, 1 April 2021.
21. FISCHER Fuel Cell Compressor, AG. Data Sheet EMTC-150k. Available online: www.fischer-fuelcell-compressor.com (accessed on 11 April 2022).
22. Tiainen, J.; Jaatinen-Värri, A.; Grönman, A.; Fischer, T.; Backman, J. Loss development analysis of a micro-scale centrifugal compressor. *Energy Convers. Manag.* **2018**, *166*, 297–307. [CrossRef]
23. Rotrex. EK10AA Datasheet. Available online: www.rotrex.com (accessed on 11 April 2022).
24. Marelli, S.; Carraro, C.; Marmorato, G.; Zamboni, G.; Capobianco, M. Experimental analysis on the performance of a turbocharger compressor in the unstable operating region and close to the surge limit. *Exp. Therm. Fluid Sci.* **2014**, *53*, 154–160. [CrossRef]
25. Müller, D. Einfluss der Anordnung und des Betriebs von Abgasturboladern auf deren Pumpgrenze. Ph.D. Thesis, Gottfried Wilhelm Leibniz Universität, Hannover, Germany, 2008.
26. Schröter, J.; Steinbarth, D.; Bauer, C.; Reichmann, U.; Kallo, J.; Willich, C. Climate and Pressure Chamber for Simulation of Flight Conditions. Available online: https://oparu.uni-ulm.de/xmlui/bitstream/handle/123456789/38074/Climate_chamber.pdf?sequence=1&isAllowed=y (accessed on 11 April 2022).